MPC Implementation of a Quasi-Time-Optimal Speed Control for a PMSM Drive, With Inner Modulated-FS-MPC Torque Control

Esteban Fuentes, César A. Silva, *Member, IEEE*, and Ralph M. Kennel, *Senior Member, IEEE*

***Abstract*—In this paper, model-predictive control is used as a framework for implementing a quasi-time-optimal speed controller for a permanent-magnet synchronous motor. The scheme consists of an inner predictive torque control, which makes use of the full actuation range provided by a two-level voltage source inverter, although with the use of pulsewidth modulation. An outer speed controller, based on classical results for the time-optimal control of the double integrator, constitutes a good example application of the proposed torque controller. The overall scheme achieves both fast transient dynamics (as fast as the physics of the system and the control constraints allow) and acceptable steady-state performance.**

***Index Terms*—Model-predictive control (MPC), permanent-magnet motors, time-optimal control, torque and speed control.**

I. Introduction

MODEL-PREDICTIVE control (MPC) techniques are gaining significant attention from the power electronics and electric drives research community, due to their high dynamic response and to the availability of sufficiently powerful digital controllers to implement them. These techniques have shown high potential for two types of applications. First one is in large power drives that operate at low switching frequency. In this type of applications, linear controllers result in very low-current control bandwidth and MPC offers a way to improve the dynamic performance without increasing the switching frequency. In this context, to achieve good steady-state performance using variants of the MPC technique is challenging, although significant progress has been made [1]–[4]. Second one is in servo drives, where there are no stringent restrictions on the switching frequency; MPC current control may be used to maximize the dynamic response of current or torque controllers, thus allowing improved dynamic response of the mechanical loops [5], [6].

One commonly used alternative for current control on servo drives is dead-beat control. This is a linear technique that is related to the MPC paradigm [7]–[9]. Dead-beat control is usually regarded as sensitive to model mismatch due to parameter estimation errors, which have detrimental effects on the performance of the loop [8]. In [9], the variations in the parameters on a permanent-magnet synchronous motor (PMSM) are dealt-with by measuring their effect on the di/dt, i.e., identifying online the relevant parameters of the system and including this information on a predictive model, achieving robust performance of the standard dead-beat control technique, despite parameter changes. This predictive control achieves excellent dynamic performance and accurate steady-state reference tracking by inverting the plant model subject to actuations within the linear modulation region. On the other hand, the finite-set MPC (FS-MPC) method [10], [11], which is based on the optimization of a cost function, rather than on a direct inversion of the plant, may be used to optimize the voltage actuation including the effect of voltage saturation, and hence maximizing the dynamic response of internal current loops, even during large transients. Due to its reliance on a machine model for the predictions, the FS-MPC method is also affected by model inaccuracies. Nevertheless, for the model-predictive direct-current-control variant, in [12], it has been shown theoretically that the technique is robust at least in the sense of convergence to a bounded region around the reference if sufficiently actuation capability is available. One drawback of the FS-MPC techniques is that they result in larger switching ripple than techniques that include pulse width modulation (PWM) voltages modulation at similar switching frequencies [11] and that they may result in a steady-state error [13] i.e., the average current may converge to a region around the reference, but not exactly to the reference. Therefore, these issues need to be addressed before the MPC technique is of practical industrial interest and much research efforts have been directed to these problems.

In this work, an MPC technique with PWM is proposed to achieve an inversion of the full electrical model, including the *back-emf* effect, when the optimal voltage actuation is in the linear modulation region. Due to the complexity of the complete machine electrical model, such inversion is not performed analytically. The current response is, instead, calculated for all the discrete possible actuations, as is done in FS-MPC. Outside the linear modulation region, these discrete actuations are used. On the other hand, in the linear modulation region, an accurate voltage actuation is derived from the predicted current error as a weighted average of the two optimal active-voltage vectors form the finite-set and the zero-voltage vector, as in

Manuscript received May 30, 2015; revised November 15, 2015; accepted December 15, 2015. Date of publication January 19, 2016; date of current version May 10, 2016.

E. Fuentes and R. M. Kennel are with the Electric Drives and Power Electronics Group, Technical University of Munich, 80333 Munich, Germany (e-mail: esteban.fuentes@tum.de; ralph.kennel@tum.de).

C. A. Silva is with the Electronics Engineering Department, Universidad Técnica Federico Santa María and with the Centro Científico y Tecnológico de Valparaíso (CCTVal), Valparaíso 239-0123, Chile (e-mail: cesar.silva@usm.cl).

Digital Object Identifier 10.1109/TIE.2016.2519326

space vector modulation. This alleviates the issues of steady-state performance and error in FS-MPC. The accuracy of the actuation still depends, however, on the accuracy of the model and errors in the parameters will affect its performance in a similar fashion as in FS-MPC schemes. Related techniques have been proposed in [14]–[16] for a multiphase drive, a multilevel converter feeding an resistive-inductive load, and for a conventional three phase VSI in an active rectifier application, respectively. Although the results in [14]–[16] show a major improvement with respect to the steady-state performance of FS-MPC without sacrificing its transient response, the underlying theoretical justification is not clear and these methods are difficult to generalize. In [14], the modulation is performed between one active vector and a zero vector, reaching only an approximate solution of the optimal actuation voltage. In [15], single-phase modulation between two voltage levels in each phase is implemented, effectively reaching the three-phase required voltage, but the neutral interaction is not considered, i.e., reducing the actuation capability. In [16], an extension to a three-phase problem is presented, but the measure of absolute current error is used to calculate duty cycles, which we believe is not the most adequate way for a three-phase system, better represented in the complex plane. In this work, the implementation of a PWM–MPC control algorithm is presented for three-phase systems, using the vector modulation formulation as a framework to calculate the optimal actuation from finite-set current error predictions. Furthermore, in this work, it will be argued that, although time varying due to changes in angular position, speed, and inductance (as a function of the angular position), the machine model is indeed linear during one sampling period, and therefore, the proposed averaging in the complex plane is an accurate method to calculate the ideal voltage actuation for the control of the current or torque. Consistent with the linearity assumption, in the linear modulation region, the issues of robustness should be similar to dead-beat control, for which solutions already exist in literature (see [9]).

To make full use of the optimal dynamic response of the internal torque loop, a quasi-optimal outer speed loop is proposed. This outer loop is time-optimal in the sense that a bang–bang torque actuation is assumed ensuring that the time to reach the speed reference is minimum [17]–[19]. Nevertheless, as it is well known, a bang–bang actuation results in chattering when the reference is reached and therefore a linear controller is use to replace it in the vicinity of the reference; hence, the technique is quasi-optimal. The performance of the technique is evaluated with experimental results in a 2.2-kW machine, as well as in simulation. The results are in good accordance with the expected ideal optimal response. The complete control algorithm is programmed on a laboratory control platform based in an Intel Pentium processor and peripherals built around an FPGA board. The PWM carrier frequency is of 11 kHz and the sampling is performed twice per period, showing that the computational load of the method is not excessive.

This paper is organized as follows. In Section II, a model of the drive is derived. The modulated FS-MPC torque control and the quasi-time-optimal speed-control (QTOSC) strategies are developed in Sections III and IV. Experimental results and general conclusion are presented in Sections V and VI, respectively.

II. Drive Model

A. PMSM

A model for the relevant dynamics of the PMSM is obtained applying Faraday's law to the stator windings. This leads to the following ordinary differential equation [20]:

$$\frac{d\boldsymbol{i}_s}{dt} = L_s^{-1}\left(\boldsymbol{v}_s - r_s\boldsymbol{i}_s - \frac{dL_s}{d\theta}\omega\boldsymbol{i}_s - J\omega\boldsymbol{\psi}\right) \tag{1}$$

where $\boldsymbol{i}_s = [i_\alpha\ i_\beta]^T$ and $\boldsymbol{v}_s = [v_\alpha\ v_\beta]^T$ are the stator current and voltage, ω and θ are the speed and position of the rotor. For convenience, these are expressed in electrical radians, i.e., $\theta = p\theta^{\{\text{mechanical}\}}$, where p is the pole pair number. The stator inductance changes with rotor position. This effect may be due to built-in rotor anisotropy, as a result of magnets buried or inserted in the rotor core or as a result of core saturation due to the main flux. In any case, the result is a dependency of the stator self-inductance L_s on θ, $L_s = T^{-1}\left[\begin{smallmatrix} L_d & 0 \\ 0 & L_q \end{smallmatrix}\right] T$, with $T = \left[\begin{smallmatrix} \cos(\theta) & \sin(\theta) \\ -\sin(\theta) & \cos(\theta) \end{smallmatrix}\right]$. Parameters L_d and L_q are the equivalent inductances in the direction of the magnet flux and the quadrature direction, respectively. Parameter r_s is the stator resistance, $J = \left[\begin{smallmatrix} 0 & -1 \\ 1 & 0 \end{smallmatrix}\right]$ and $\boldsymbol{\psi} = T^{-1}\left[\begin{smallmatrix} \psi_m \\ 0 \end{smallmatrix}\right]$ is the flux produced by the rotor magnet, of magnitude ψ_m.

The torque generated by the PMSM is given by

$$T_e = \frac{3}{2}p(\psi_m i_q + (L_d - L_q)i_d i_q) \tag{2}$$

with $\left[\begin{smallmatrix} i_d \\ i_q \end{smallmatrix}\right] = T\boldsymbol{i}_s$.

The model of the drive is completed with the dynamics of the mechanical variables [21]

$$\frac{d}{dt}\begin{bmatrix}\omega \\ \theta\end{bmatrix} = \begin{pmatrix}\frac{p}{J_m}(T_e - T_l) \\ \omega\end{pmatrix} \tag{3}$$

where J_m and T_l represent the inertia of the drive and the load torque.

B. Maximum Torque Per Ampere Operation

Minimization of losses is a feature desirable in every drive application. In a PMSM drive, maximum torque per ampere (MTPA) operation defines two regimes.

1) At low speed, a proper balance between the two torque components: 1) by interaction between stator currents; and 2) rotor magnet flux and reactance torque, enables the generation of an arbitrary torque value (within the stator currents constraint) minimizing Joule losses.
2) At high speed, flux weakening is required to produce torque and at the same time respect the input voltage constraint.

In this work, we focus on the first case, where MTPA operation is achieved when the stator currents satisfy

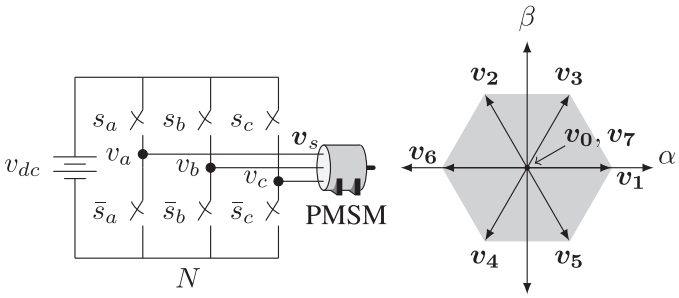

Fig. 1. VSI (left) and synthesized voltages in the $\alpha\beta$-plane (right).

$$i_d + \frac{L_d - L_q}{\psi_m}\left(i_d^2 - i_q^2\right) = 0\,. \tag{4}$$

Equation (4) is used as one of the control targets, defined formally by (12) in Section II-C. If operating on the field weakening region is a requirement, an additional target should be specified for the case when the speed surpasses the base speed threshold.

C. Actuator–Voltage Source Inverter

The stator voltage $\boldsymbol{v}_s$ constitutes the input of our system and is, in this work, synthesized using a two-level voltage source inverter (VSI). This converter is depicted in Fig. 1.

The use of PWM establishes a relationship between $\boldsymbol{v}_s$, the duty cycle applied on each of its three legs d_a, d_b, and d_c, and the dc-link voltage v_{dc}

$$\boldsymbol{v}_s = \frac{2}{3} v_{\mathrm{dc}} \begin{bmatrix} 1 & -1/2 & -1/2 \\ 0 & \sqrt{3}/2 & -\sqrt{3}/2 \end{bmatrix} \begin{bmatrix} d_a \\ d_b \\ d_c \end{bmatrix} \tag{5}$$

with $d_{\{a,b,c\}} \in [0,1]$, generating an hexagon in the $\alpha\beta$-plane. The vertices of the hexagon correspond to the voltage vectors the VSI generates, when the active switching states are applied. The VSI also generates two zero vectors. In the following, the switching states are referred to as $\boldsymbol{v}_0, \boldsymbol{v}_1, \ldots, \boldsymbol{v}_7$, where the index is the decimal representation of the corresponding switching state, encoded in binary as $s_c s_b s_a$. Given the sampling period h, the duty cycle defines the portion of h in which the corresponding switch remains on

$$s_x(t) = \begin{cases} 1, \text{ if } (t/h \bmod 1) \le d_x \\ 0, \text{ if } (t/h \bmod 1) > d_x. \end{cases} \tag{6}$$

In this way, the mean value of the corresponding voltage v_i in one sampling period h can take any value in $[0, v_{\mathrm{dc}}]$.

The gray area inside the hexagon in Fig. 1 constitutes the actuation set for the proposed controller. The purpose of the later, and particularly of the proposed inner torque controller, is to generate the duty cycles d_a, d_b, and d_c that lead the T_e toward its reference, respecting the MTPA operation condition in (4).

III. Torque Control

Consider the control of a simple integrator

$$\frac{dx}{dt} = \frac{1}{\tau} u \tag{7}$$

if we assume a ZOH input, we can describe the system dynamics with the discrete time model

$$x[n+1] = x[n] + \frac{h}{\tau} u[n]. \tag{8}$$

If we also assume the constraint $u \in [-\hat{u}, \hat{u}]$, then a state feedback rule that steers x to the origin in minimum time (steps) and ensures maximum utilization of the actuation range is given by

$$u = \pi(x) = \begin{cases} -\frac{\tau}{h} x, & \text{if } |x| \le \frac{h}{\tau}\hat{u} \\ -\mathrm{sgn}(x)\hat{u}, & \text{if } |x| > \frac{h}{\tau}\hat{u}. \end{cases} \tag{9}$$

This feedback rule gives exactly the actuation required to steer x to the origin in one step, when the current state is close enough to the origin, i.e., when the resulting actuation is inside the actuation range $[-\hat{u}, \hat{u}]$. Otherwise, its output has maximum magnitude and the sign that will steer x in the direction of the origin.

This approach is not very useful, when the purpose is to control the torque in a PMSM drive, since it requires an inversion of the system dynamics. This is not an easy task in the case of the PMSM, which is a nonlinear multivariable system. Still, it provides a good overview of the task at hand.

As in any control problem, the key point is the *inversion*, which in this work is achieved through a linear approximation of the dynamics. Two important elements for this point are the discrete-time description of the system dynamics and the definition of a *target*, which will play the role of the reference (the origin in the simple integrator example).

A. Discrete-Time Model

A discrete-time version of the stator windings dynamics is obtained with the forward-Euler discretization rule

$$\boldsymbol{i}_s[n+1] = f(x,u) \tag{10}$$

$$= \boldsymbol{i}_s[n] + h \left.\frac{d\boldsymbol{i}_s}{dt}\right|_{t=hk} \tag{11}$$

where $\boldsymbol{x} = [\boldsymbol{i}_s\ \omega\ \theta]^T$, $u = \boldsymbol{v}_s$, and the derivative of $\boldsymbol{i}_s$ is given by (1).

B. Target

We define the target as a function of the predicted stator currents

$$\boldsymbol{e} = g(\boldsymbol{i}_s) = \begin{pmatrix} T_e - T_e^* \\ i_d + \frac{L_d - L_q}{\psi_m}\left(i_d^2 - i_q^2\right) \end{pmatrix}. \tag{12}$$

In steady state, we would like to reach $e = \mathbf{0}$. Since we are interested in the value of the torque in the next sampling instant, the rotation to the dq frame is performed with the angle

$$\theta[n+1] = \theta[n] + h\omega[n]. \tag{13}$$

C. Predictive Torque Control

The composed function $(g \circ f)(\boldsymbol{x}[n], \boldsymbol{u})$ maps points in the actuation space (voltage vectors in the $\alpha\beta$-plane) to state predictions in the $e_{T_e} e_{i_d}$-plane, for an initial condition $\boldsymbol{x}[n]$. An inversion of this function would provide us with the actuation required to reach the target (torque reference tracking, plus MTPA operation) in the next sampling instant. Finding such an inverse is, however, not trivial, specially if we ought to consider the constraints on $\boldsymbol{u}$ ($\boldsymbol{v}_s$), imposed by the VSI. This complications are avoided by using a linear approximation and interpolation as shown in Fig. 2. This figure shows that predictions form a hexagon in the $e_{T_e} e_{i_d}$-plane. The *target* is the origin of this plane $[e_{T_e},\, e_{i_d}]^T = \mathbf{0}$. In plot (a), operation on the linear modulation region is shown. Here, the target is inside the hexagon and is achieved by a linear combination of predictions $\boldsymbol{e}_2$, $\boldsymbol{e}_3$, and $\boldsymbol{e}_0$. In plot (b), the target lies outside the hexagon. This corresponds to overmodulation operation. In this case, the best the controller can do is to approach the target through a linear combination of predictions $\boldsymbol{e}_2$ and $\boldsymbol{e}_3$ to reach the point on the intersection between the boundary of the hexagon and the line between $\boldsymbol{e}_0$ and the target. In broad terms, the proposed algorithm works as follows.

1) Predictions in the $e_{T_e} e_{i_d}$-plane are calculated for the voltage vectors produced by all the feasible switching configurations in the VSI

$$\boldsymbol{e}_i = (g \circ f)(\boldsymbol{x}[n], \boldsymbol{v}_i) \quad \text{with } i = 0, \ldots, 6\,. \tag{14}$$

They are understood as vectors in the $e_{T_e} e_{i_d}$-plane.

2) The pair of adjacent predictions $\boldsymbol{e}_a$ and $\boldsymbol{e}_b$, i.e., $(a, b) \in \{(2,3), (3,1), (1,5), (5,4), (4,6), (6,2)\}$, which linearly combined with $\boldsymbol{e}_0$ to reach the target is found checking the condition

$$\begin{aligned} m(\boldsymbol{e_a}, \boldsymbol{e_b}) = &\{((\boldsymbol{e}_a - \boldsymbol{e}_0) \times (-\boldsymbol{e}_0)) \\ &\cdot ((\boldsymbol{e}_b - \boldsymbol{e}_0) \times (-\boldsymbol{e}_0)) \leq 0\} \\ \wedge\ &\{(\boldsymbol{e}_a - \boldsymbol{e}_0) \cdot (-\boldsymbol{e}_0) > 0\} \\ \wedge\ &\{(\boldsymbol{e}_b - \boldsymbol{e}_0) \cdot (-\boldsymbol{e}_0) > 0\}\,. \end{aligned} \tag{15}$$

A linear combination of $\boldsymbol{e}_a$, $\boldsymbol{e}_b$, and $\boldsymbol{e}_0$ maps a triangle in the $e_{T_e} e_{i_d}$-plane. The appropriate ab pair is found when the cross product of vector $\boldsymbol{e}_a - \boldsymbol{e}_0$ and $\mathbf{0} - \boldsymbol{e}_0$ has the inverse sign of the cross product between $\boldsymbol{e}_b - \boldsymbol{e}_0$ and $\mathbf{0} - \boldsymbol{e}_0$ and the projections of vector $\mathbf{0} - \boldsymbol{e}_0$ on $\boldsymbol{e}_a - \boldsymbol{e}_0$ and $\boldsymbol{e}_b - \boldsymbol{e}_0$ are both positive, i.e., condition $m(\cdot)$. This is depicted in Fig. 2, where vectors $\boldsymbol{e}_a$ and $\boldsymbol{e}_b$ are $\boldsymbol{e}_2$ and $\boldsymbol{e}_3$, respectively.

3) The linear combination to reach the target is found solving $\boldsymbol{d}' = [d'_a\ d'_b]^T$ from

$$[(\boldsymbol{e}_a - \boldsymbol{e}_0)\ (\boldsymbol{e}_b - \boldsymbol{e}_0)]\boldsymbol{d}' = -\boldsymbol{e}_0 \tag{16}$$

where $\boldsymbol{e}_a$ and $\boldsymbol{e}_b$ are two predictions which satisfy $m(\boldsymbol{e}_a, \boldsymbol{e}_b)$.

4) The constraint on $\boldsymbol{v}_s$ is taken into account with

$$\begin{bmatrix} d_a \\ d_b \end{bmatrix} = \begin{cases} \boldsymbol{d}', & \text{if } d'_a + d'_b \leq 1 \\ \frac{1}{d'_a + d'_b} \boldsymbol{d}', & \text{if } d'_a + d'_b > 1. \end{cases} \tag{17}$$

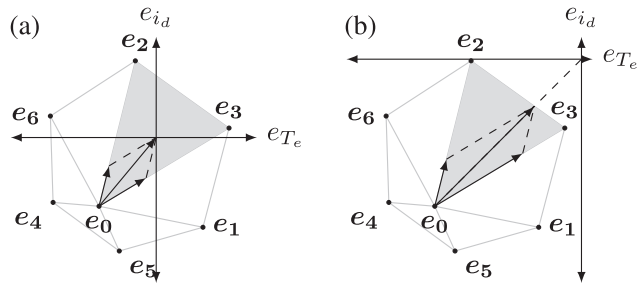

Fig. 2. Pulsewidth-modulation scheme for the inner torque controller.

This produces a voltage vector, which lays on the constraint imposed by the VSI, i.e., the gray hexagon in Fig. 1.

5) The voltage vector to be applied is then given by

$$\boldsymbol{v}_s^* = d_a \boldsymbol{v}_a + d_b \boldsymbol{v}_b. \tag{18}$$

The reference voltage vector $\boldsymbol{v}_s^*$ can be then synthesized using standard PWM techniques, such as space vector modulation.

Note that in this form, the feedback rule resembles the feedback rule for the simple integrator introduced in (9). The linear approximation and interpolation gives an approximate system inversion and the operation in (17) takes the constraint into account. The linear approximation is valid, as long as the sampling period is small, compared to the time constants involved in the variations of θ and ω, the variables behind the nonlinearities in the stator windings dynamics.

Fig. 3 presents a flowchart of the proposed torque control algorithm. The later is specified with the *predictive model* $f(\cdot)$, and function $g(\cdot)$, which amounts to a change in variables. The actuation set in this formulation is constituted by the voltage vectors generated by the two-level VSI and $m(\cdot)$ is a boolean function that is true when $\boldsymbol{e} = \mathbf{0}$ is inside the triangle formed by $\boldsymbol{e}_0$, $\boldsymbol{e}_i$, and $\boldsymbol{e}_{i-1}$ in the plane of the components of $\boldsymbol{e}$, in this case, $\boldsymbol{e_{T_e} e_{i_d}}$.

D. Torque Control Results

Fig. 4 presents simulation and experimental results using the proposed torque control scheme. The results are in both situations very similar, and the control system behaves as expected. The experimental results do now show the intersample current and torque ripple, but their form is very predictable and is given by the PWM technique used. The dots in plots (a), (b), and (c) represent the sampled measurements.

In the simulations, the rotor speed and angle at $t = 0$ (s) are $\omega = 2\pi \cdot 30$ (rad$^{\text{e}}$) and $\theta = 0$ (rad$^{\text{e}}$). The sampling period for the controller is $h = 50$ (μs). The ripple observed in the current is produced by the space vector modulation: with $\theta = 0$ (rad$^{\text{e}}$), the q-axis is aligned with the β-axis and the controller alternates between v_3 and v_2 to make the stator current grow along the MTPA curve, up to the stator current magnitude constraint represented in plots (c) and (f) with dashed and dotted gray line, respectively. The space vector modulation (SVM) is implemented using a PWM scheme with triangular carriers.

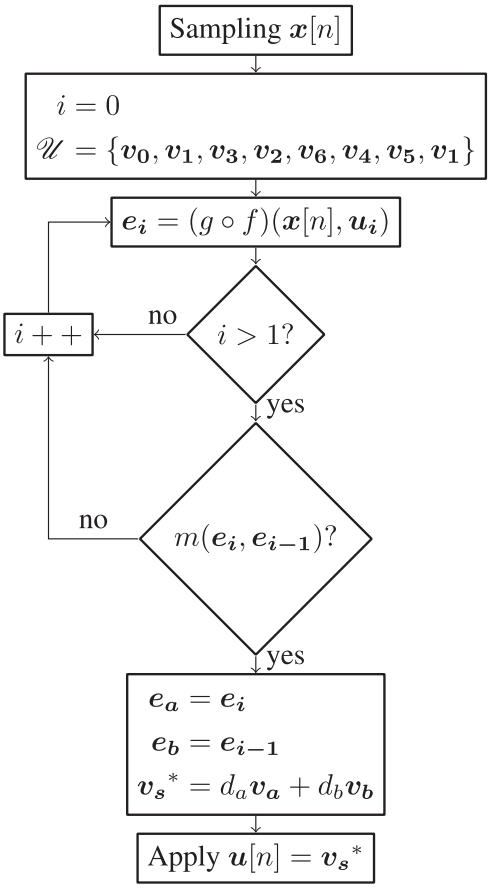

Fig. 3. Flowchart for the proposed torque control algorithm.

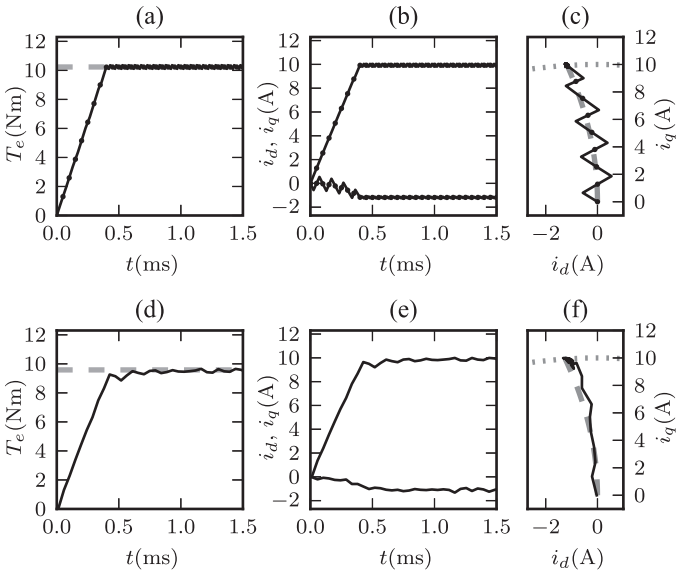

Fig. 4. (a), (b), (c) Simulation and (d), (e), (f) experimental results for the torque control of the PMSM with the proposed scheme.

Sampling occurs at the extreme values of the carrier, so that the current measurements (marked with points) correspond to their mean value. With this, the controller does not *see* the ripple. For the experimental test, the sampling period for the controller is $h = 46.1$ (μs) and at $t = 0$, the rotor is at rest.

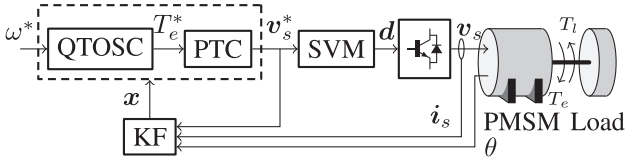

Fig. 5. Control scheme: QTOSC for the PMSM.

IV. Speed Control

In [19], it was shown how a QTOSC for the PMSM could be implemented using the FS-MPC algorithm, as presented in [22], through the use of a specially designed cost function. The synthesis of the later was enabled by two considerations:

1) Use of a convenient approximation for the relevant system dynamics: the double integrator;
2) Use of widely known results in optimal control theory, namely, the time-optimal control of the double integrator [23].

These are also exploited in this work. The implementation of the controller, however, takes a different form. The speed control algorithm developed in this work takes the form of a cascaded control, with the torque controller introduced in the last section as inner controller and the speed controller introduced in this section, the QTOSC, as outer controller. Fig. 5 presents a scheme of the whole control system. The scheme considers the use of a Kalman filter to estimate the system state and, in particular, ω and T_l. For more details on this filter, see below.

From the speed reference and the estimated (filtered) state, the QTOSC calculates the torque reference which is the input for the predictive toque control (PTC) algorithm. The PTC outputs the reference for the stator voltage $\boldsymbol{v}_s^*$, which is transformed to duty cycles by the SVM block. The whole controller uses the state feedback $\boldsymbol{x}$, synthesized by the Kalman filter, out of the measurements of the rotor angle θ and the stator currents $\boldsymbol{i}_s$.

Two aspects from the time-optimal control of the double integrator are important for the proposed controller.

1) The time-optimal controller is a *ban–bang* controller [17], [18]: the actuation takes its maximum value for every point in the state space. The introduction of constraints turns the controller into a *bang-zero-bang* controller: $u = 0$ once the constraint is achieved.
2) The time-optimal controller introduces a partition of the state space, defining two regions. The boundary between these regions is known as the switching curve, or Γ curve. The position of the state with respect to this curve defines the sign for the actuation.

Note that the assumption of a *bang–bang* structure does not hold for discrete-time systems [24]. In this work, continuous-time results are approximated using a smoothening approach.

A. System Dynamics Approximation

The use of the CS-MPC algorithm as inner torque controller, together with the assumption on the bang–bang structure for the actuation, enables the approximation of the torque dynamics by

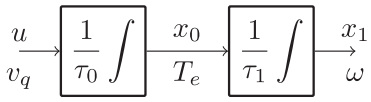

Fig. 6. Double integrator representation of the motor mechanical dynamics.

those of a simple integrator, as in (7), being controlled with the feedback rule (9). That is, to model the torque dynamics, we can take

$$\frac{dx_0}{dt} = \frac{1}{\tau_0}u \tag{19}$$

with $x_0 = T_e$ and $\tau_0 = \frac{2L_q}{3p\psi_m}$. The actuation u represents the stator voltage in the direction that increases T_e: if $L_d \approx L_q$, as is the case in surface-mounted PMSMs, the q-direction. Note that for the speed controller design, we do not need to calculate this direction, the inner torque controller takes care of it and also of compensating all the effects neglected by this approximation: *back-emf*, stator winding resistance, etc.

The speed dynamics are approximated with

$$\frac{dx_1}{dt} = \frac{1}{\tau_1}x_0 \tag{20}$$

with $x_1 = \omega$ and $\tau_1 = J_m$.

Fig. 6 depicts the double integrator approximation. In the following, we will assume that the goal is to control this system to reach the origin $x_1 = x_0 = 0$. In order to reach an arbitrary reference for x_1 and compensate for the load torque, we only need to displace the origin in x_1 and x_0, respectively,

$$\begin{bmatrix} x_0' \\ x_1' \end{bmatrix} = \begin{bmatrix} x_0 - T_l \\ x_1 - \omega^* \end{bmatrix}. \tag{21}$$

In summary, the dynamics of the double integrator are given by

$$\frac{d\boldsymbol{x}}{dt} = \begin{pmatrix} \frac{1}{\tau_0}u \\ \frac{1}{\tau_1}x_0 \end{pmatrix} \tag{22}$$

with $x = [x_0\ x_1]^T$. A discrete-time state-space model

$$\boldsymbol{x}[n+1] = f(\boldsymbol{x}[n], u[n]) \tag{23}$$

is obtained through a Taylor series expansion of the solution of (22)

$$f(\boldsymbol{x}, u) = \begin{pmatrix} x_0 + \frac{h}{\tau_0}u \\ x_1 + \frac{h}{\tau_1}x_0 + \frac{h^2}{2\tau_1\tau_0}u \end{pmatrix} \tag{24}$$

where h is the sampling period.

It is clear that the double integrator is a rough approximation of the real system dynamics. However, it must be noted that the most significant terms in the response of T_e and ω, considering the aforementioned neglected effects, to a step in v_q, match the step response of the double integrator. That is, the double integrator is a valid approximation for the transients of the motor.

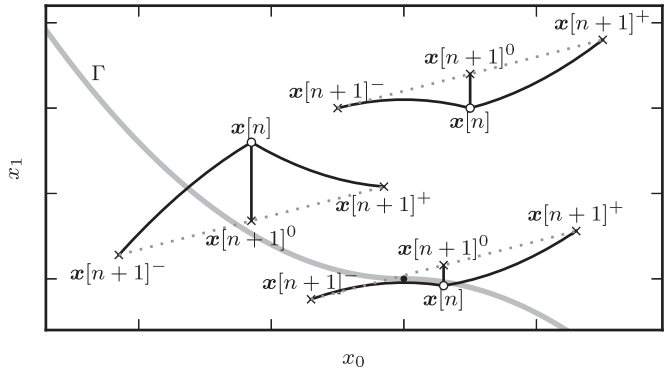

Fig. 7. Representation of the proposed control algorithm in the $x_0 - x_1$-plane.

B. Quasi-Time-Optimal Control for the Double Integrator

The classical result asserts that, in continuous time and under the assumption of a constrained actuation $u \in [-\hat{u}, \hat{u}]$, time-optimal control for the double integrator is achieved fixing u to one of its extreme values, with sign given by the position of the state with respect to the curve

$$\Gamma: \quad x_1 + \mathrm{sgn}(x_0)\tau x_0^2 = 0 \tag{25}$$

with $\tau = \frac{\tau_0}{2\tau_1\hat{u}}$. This curve corresponds to the system trajectories obtained when, starting from the origin, maximum actuation is applied to the system, with the time running backward. In continuous time, the time-optimal controller steers the system toward the Γ curve and, once it is reached, the sign of the actuation is inverted, until the origin is reached.

Fig. 7 represents different initial conditions $\boldsymbol{x}[n]$, state predictions $\boldsymbol{x}[n+1]$ using $u \in \{-\hat{u}, 0, \hat{u}\}$, all the points reachable with $u \in [-\hat{u}, \hat{u}]$ as dotted lines and the Γ curve in gray. The later is approached giving as reference for the inner x_0 (T_e) controller, the point where the line in dotted gray cuts Γ. Once the desired steady state is approached, a linear smooth controller takes over, in order to avoid chattering.

For the design of the speed controller for the PMSM, the constraint for the actuation is set to

$$\hat{u} = \frac{\sqrt{3}}{3}v_{\mathrm{dc}} \tag{26}$$

which corresponds to the maximum amplitude the two-level VSI can achieve, when synthesizing perfectly sinusoidal stator voltages.

1) Approaching the Switching Curve: To approximate this behavior in discrete time, we first acknowledge that, for a sampling period h and an initial condition $\boldsymbol{x}[n]$, after applying $u \in [-\hat{u}, \hat{u}]$, the system will reach a point belonging to the line between $f(\boldsymbol{x}[n], -\hat{u})$ and $f(\boldsymbol{x}[n], \hat{u})$ in the $x_0\,x_1$-plane, which belongs to the line

$$x_1 = \frac{h}{2\tau_1}x_0 + b \tag{27}$$

with

$$b = x_1[n] + \frac{h}{2\tau_1}x_0[n].$$

This is obtained by manipulating (24). The line is depicted in Fig. 7 with dotted lines for different initial conditions $\boldsymbol{x}[n]$.

This line cuts Γ at

$$x_0^\star = \operatorname{sgn}(b)\frac{h\hat{u}}{2\tau_0}\left(1-\sqrt{1+\frac{8\tau_0\tau_1}{h^2\hat{u}}|b|}\right). \tag{28}$$

This value can be feed to an inner x_0 (T_e) controller as reference to mimic the continuous-time time-optimal behavior.

2) Stator Current Constraint: In MTPA operation, a constraint for the stator currents implies a constraint in T_e, i.e., a constraint in x_0

$$x_0 \in [-\hat{x}_0, \hat{x}_0]. \tag{29}$$

In the proposed scheme, this can be enforced with

$$x_0^\diamond = \begin{cases} x_0^\star, & \text{if } |x_0^\star| \le \hat{x}_0 \\ \operatorname{sgn}(x_0^\star)\hat{x}_0, & \text{if } |x_0^\star| > \hat{x}_0. \end{cases} \tag{30}$$

3) Vicinity of the Steady State: A special treatment is required near the steady state. As depicted in Fig. 7, near the origin the line in (27) cuts Γ in the opposite quadrant of $\boldsymbol{x}[n]$ and repeatedly approaching the point where they cut generates chattering. The situation is aggravated if we consider the effects neglected by the double-integrator approximation and, furthermore, measurement noise and parameter mismatch. For this situation, the proposed method prescribes the use of a linear and more smoother controller, which makes the state approach the origin asymptotically.

If we assume that near steady state u can be manipulated to obtain

$$x_0[n+1] = x_0[n] + \frac{h}{\tau_0}u \tag{31}$$

$$= x_0^*[n] \tag{32}$$

$$= -K\frac{2\tau_1}{h}x_1[n] \tag{33}$$

i.e., the reference for x_0, x_0^* can be achieved in one sampling period and is given by a linear feedback of state x_1, where K is a tunning parameter, we can characterize the closed-loop dynamics with the difference equation

$$x_1[n+1] + (K-1)x_1[n] + Kx_1[n-1] = 0 \tag{34}$$

and use K to fix the dynamics. The damping ratio for the closed loop can be fixed at $\xi = \frac{1}{\sqrt{2}}$ with $K = 0.24498$.

In a first approach, this strategy can be imposed when the state lays inside the region

$$\mathcal{T} := \left\{\boldsymbol{x} : |x_0| < \frac{h}{\tau_0}\hat{u} \ \wedge \ |x_1| < \frac{h^2}{2\tau_0\tau_1}\hat{u}\right\}. \tag{35}$$

Points on Γ in $\mathcal{T}$ will land on the opposite quadrant of $x[n]$ with the strategy given by (30). Otherwise, this region can be adjusted according to estimates of measurement noise.

Finally, the reference for x_0 (T_e) is given by

$$x_0^* = \begin{cases} -K\frac{2\tau_1}{h}x_1, & \text{if } x \in \mathcal{T} \\ x_0^\diamond, & \text{if } x \notin \mathcal{T}. \end{cases} \tag{36}$$

C. State Estimation

As in many industrial applications, our test bench is equipped with a standard incremental encoder. The usual solution for estimating the speed consists in applying a derivator (using the backward Euler approximation) and linear filters on the measurement of θ. However, the proposed speed control strategy can be understood as a high-gain nonlinear state feedback rule and, as such, it requires a very reliable estimation of the state and, particularly, of the speed. In this scenario, the usual solution would introduce significant delay, which would result in an oscillatory response. To avoid these issues, and in order to effectively separate the control and the observation problems, a Kalman filter was used. The filter was implemented in its *reduced-order extended* form. Reduced-order, since the currents measurements are deemed reliable enough and are used directly as estimations of the state $\boldsymbol{i}_s$, and extended, because the nonlinear model

$$\frac{d}{dt}\begin{bmatrix}\boldsymbol{i}_s \\ \omega \\ \theta \\ \tilde{T}_l\end{bmatrix} = \begin{pmatrix} L_s^{-1}\left(\boldsymbol{v}_s - r_s\boldsymbol{i}_s - \frac{dL_s}{d\theta}\omega\boldsymbol{i}_s - J\omega\boldsymbol{\psi}\right) \\ \frac{p}{J_m}\left(T_e - \tilde{T}_l\right) \\ \omega \\ 0 \end{pmatrix} \tag{37}$$

is used as internal model for the filter. Note that a state equation is included for $\tilde{T}_l$. In this way, the load torque is estimated by the filter, effectively introducing integration to the speed control loop.

The tunning of the filter comprises finding estimations for the covariance of additive noise in the rotor angle measurement θ and in the state equation. In this work, the tunning was done empirically, adjusting the covariances to get a good compromise between noise rejection and convergence speed. For more details on the implementation of the filter refer to [25].

V. Results

The performance of the proposed controller was tested using an experimental setup consisting mostly of industrial components. A 2.0-kW PMSM is driven by an industrial VSI, modified for direct access to the gate signals of the IGBTs. Load torque is generated by a 2.2-kW induction machine, driven by an industrial VSI set for torque control.

The gating signals for the VSI driving the PMSM are produced by a real-time computer with an Intel processor running at a clock frequency of 1.4 GHz. Real-time operation is achieved with a Linux kernel, modified with the *real-time application interface* (RTAI) package. The control algorithm was written in C, so that the same code could be used for experimental tests and simulations. The latter were implemented in Python, with the SciPy/Numpy [26] and SClib packages [27].

Technical limitations of the test bench forced the reduction in the voltage range to produce the experimental results presented here: when modulating relatively high voltages, the zero voltage vector is applied for very short time and the noise introduced by the switching elements is very noticeable in the current measurements, which are synchronized to occur while the zero vector is applied (at the top of the triangular PWM carriers). To

TABLE I
EXPERIMENTAL SETUP PARAMETERS

$p = 3$	$J_m = 12.08 \times 10^{-3}\,(\mathrm{kgm}^2)$
$r_s = 2.2\,(\Omega)$	
$\psi_m = 0.211\,(\mathrm{Wb})$	
$L_d = 8.4\,(\mathrm{mH})$	
$L_q = 11.1\,(\mathrm{mH})$	$h = 46.088\,(\mu\mathrm{s})$

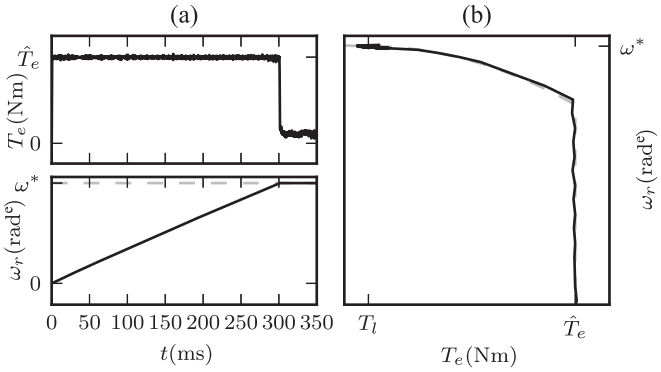

Fig. 8. Experimental results: speed step reference with the proposed scheme. The reference for the rotor speed is $\omega^* = 2\pi \cdot 150\ (\mathrm{rad^e/s})$.

tackle this, the value for the maximum actuation was set to 90% of $\hat{u}$ [see (26)].

The relevant parameters of the test bench are presented in Table I.

Figs. 8 and 9 present experimental results using the proposed control scheme. In the presented tests, the constraints for the stator currents and electrical torque are given by $\hat{i} = 10\ (\mathrm{A})$ and $\hat{T}_e = 9.58\ (\mathrm{Nm})$.

In Fig. 8, a step-change in the speed reference is presented. In plot (b), the dashed gray plot represents the Γ curve and the constraint in T_e. This plot verifies that the proposed control scheme effectively recreates the desired behavior and, at the same time, gives ground to the use of the double integrator as a valid approximation to account for the desired dynamics. Fig. 9 presents a complete maneuver including startup, load torque impact, and speed reversal.

In all the tests, the dynamic behavior matches the requirements: both the electrical torque T_e and the rotor speed ω reach their references at the same time and as fast as the physical constraints of the system allow, without compromising the steady-state performance, i.e., measurement noise is not particularly amplified once steady state is reached.

The ripple in the stator currents and electrical torque is as expected when using PWM. These variables have a concentrated frequency spectrum and unmodeled dynamics are not excited, despite the extremely stiff control achieved.

VI. CONCLUSION

The control scheme proposed in this paper effectively combines MPC and PWM techniques to achieve fast transient dynamics and acceptable steady-state performance. These concepts were used to implement a QTOSC for the PMSM. Time optimality is usually avoided as control goal, since it is known

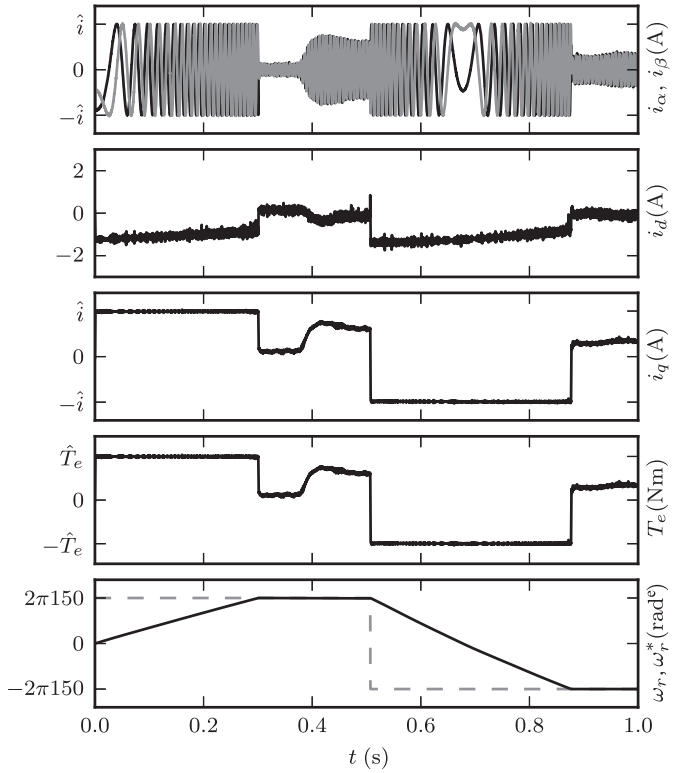

Fig. 9. Experimental results: startup ($t = 0$), load torque impact [$t \approx 0.4$ (s)], and speed reversal maneuver [$t \approx 0.5$(s)].

to produce stiff and thus unstable controllers. This work shows how such goal can be approached at a low level (torque and speed control) with relatively standard equipment.

REFERENCES

[1] T. Geyer and S. Mastellone, "Model predictive direct torque control of a five-level ANPC converter drive system," in *Proc. IEEE Energy Convers. Congr. Expo. (ECCE)*, Sep. 2011, pp. 363–370.

[2] J. Scoltock, T. Geyer, and U. Madawala, "A model predictive direct current control strategy with predictive references for mv grid-connected converters with -filters," *IEEE Trans. Power Electron.*, vol. 30, no. 10, pp. 5926–5937, Oct. 2015.

[3] T. Geyer and D. Quevedo, "Performance of multistep finite control set model predictive control for power electronics," *IEEE Trans. Power Electron.*, vol. 30, no. 3, pp. 1633–1644, Mar. 2015.

[4] M. Jofre and C. Silva, "Low switching frequency explicit model predictive control of induction machines fed by an NPC," in *Proc. IEEE Int. Symp. Ind. Electron. (ISIE)*, Jun. 2014, pp. 836–841.

[5] M. Preindl and S. Bolognani, "Model predictive direct speed control with finite control set of PMSM-VSI drive systems," in *Proc. IEEE Predict. Control Elect. Drives Power Electron. (PRECEDE 2011)*, Oct. 2011, pp. 17–23.

[6] X. Lin-Shi, F. Morel, A. Llor, B. Allard, and J.-M. Retif, "Implementation of hybrid control for motor drives," *IEEE Trans. Ind. Electron.*, vol. 54, no. 4, pp. 1946–1952, Aug. 2007.

[7] M. Kazmierkowski and L. Malesani, "Current control techniques for three-phase voltage-source PWM converters: A survey," *IEEE Trans. Ind. Electron.*, vol. 45, no. 5, pp. 691–703, Oct. 1998.

[8] J.-F. Stumper, V. Hagenmeyer, S. Kuehl, and R. Kennel, "Flatness-based deadbeat control revisited: Robust and high-performance design for electrical drives," in *Proc. IEEE Amer. Control Conf.*, Jun. 2013, pp. 1822–1827.

[9] J. Weigold and M. Braun, "Predictive current control using identification of current ripple," *IEEE Trans. Ind. Electron.*, vol. 55, no. 12, pp. 4346–4353, Dec. 2008.

[10] M. Preindl and S. Bolognani, "Model predictive direct speed control with finite control set of PMSM drive systems," *IEEE Trans. Power Electron.*, vol. 28, no. 2, pp. 1007–1015, Oct. 2013.
[11] J. Rodriguez, R. Kennel, J. Espinoza, M. Trincado, C. Silva, and C. Rojas, "High-performance control strategies for electrical drives: An experimental assessment," *IEEE Trans. Ind. Electron.*, vol. 59, no. 2, pp. 812–820, Feb. 2012.
[12] T. Geyer, R. Aguilera, and D. Quevedo, "On the stability and robustness of model predictive direct current control," in *Proc. IEEE Int. Conf. Ind. Technol. (ICIT)*, Feb. 2013, pp. 374–379.
[13] P. Lezana, R. Aguilera, and D. Quevedo, "Steady-state issues with finite control set model predictive control," in *Proc. 35th Annu. Conf. IEEE Ind. Electron. Soc. (IECON)*, Nov. 2009, pp. 1776–1781.
[14] F. Barrero, M. Arahal, R. Gregor, S. Toral, and M. Duran, "One-step modulation predictive current control method for the asymmetrical dual three-phase induction machine," *IEEE Trans. Ind. Electron.*, vol. 56, no. 6, pp. 1974–1983, Jun. 2009.
[15] L. Tarisciotti, P. Zanchetta, A. Watson, S. Bifaretti, and J. Clare, "Modulated model predictive control for a seven-level cascaded h-bridge back-to-back converter," *IEEE Trans. Ind. Electron.*, vol. 61, no. 10, pp. 5375–5383, Oct. 2014.
[16] L. Tarisciotti, P. Zanchetta, A. Watson, J. Clare, M. Degano, and S. Bifaretti, "Modulated model predictive control for a three-phase active rectifier," *IEEE Trans. Ind. Appl.*, vol. 51, no. 2, pp. 1610–1620, Apr./Mar. 2015.
[17] L. Pontryagin and L. Neustadt, *The Mathematical Theory of Optimal Processes*. New York, NY, USA: Gordon and Breach, 1962, no. Bd. 4.
[18] C. Y. Kaya, S. K. Lucas, and S. T. Simakov, "Computations for bang–bang constrained optimal control using a mathematical programming formulation," *Optim. Control Appl. Methods*, vol. 25, no. 6, pp. 295–308, Jan. 2004.
[19] E. Fuentes, D. Kalise, J. Rodriguez, and R. Kennel, "Cascade-free predictive speed control for electrical drives," *IEEE Trans. Ind. Electron.*, vol. 61, no. 5, pp. 2176–2184, May 2014.
[20] D. Paulus, P. Landsmann, and R. Kennel, "Sensorless field- oriented control for permanent magnet synchronous machines with an arbitrary injection scheme and direct angle calculation," in *Proc. IEEE Symp. Sensorless Control Elect. Devices (SLED)*, Sep. 2011, pp. 41–46.
[21] S. Villwock and M. Pacas, "Application of the Welch-method for the identification of two- and three-mass-systems," *IEEE Trans. Ind. Electron.*, vol. 55, no. 1, pp. 457–466, Jan. 2008.
[22] J. Rodriguez *et al.*, "Predictive current control of a voltage source inverter," *IEEE Trans. Ind. Electron.*, vol. 54, no. 1, pp. 495–503, Feb. 2007.
[23] V. Rao and D. Bernstein, "Naive control of the double integrator," *IEEE Control Syst. Mag.*, vol. 21, no. 5, pp. 86–97, Oct. 2001.
[24] D. Chen, L. Bako, and S. Lecoeuche, "The minimum-time problem for discrete-time linear systems: A non-smooth optimization approach," in *Proc. IEEE Conf. Control Appl. (CCA)*, Oct. 2012, pp. 196–201.
[25] E. Fuentes, C. Silva, and J. Yuz, "Predictive speed control of a two-mass system driven by a permanent magnet synchronous motor," *IEEE Trans. Ind. Electron.*, vol. 59, no. 7, pp. 2840–2848, Jul. 2012.
[26] E. Jones *et al.* (2001). *SciPy: Open Source Scientific Tools for Python* [Online]. Available: http://www.scipy.org/
[27] E. Fuentes and H. E. Martinez, "SClib, A hack for straightforward embedded C functions in Python," arXiv e-prints 1412.6395, Dec. 2014[Online]. Available: https://github.com/drestebon/SClib

Esteban Fuentes received the M.S. degree in electronic engineering from the Technical University Federico Santa María (UTFSM), Valparaíso, Chile, in 2009, and the Dr.-Ing. degree from the Technical University of Munich (TUM), Munich, Germany, in 2015, where he continues to work on applications of optimal control theory in drives and power electronics.

César A. Silva (S'01–M'02) received the B.Eng. degree in electronic engineering from the Universidad Ténica Federico Santa María (UTFSM), Valparaíso, Chile, in 1998 and the Ph.D. degree in 2003, where he was granted the Overseas Research Students Awards Scheme to join as a postgraduate research student at the Power Electronics Machines and Control Group, University of Nottingham, U.K., in 1999.

Since 2002, he is currently Associate Professor with the Departamento de Electrónica, UTFSM, Chile. He teaches electric machines theory, power electronics, and ac machine drives. His main research interests include sensorless vector control of ac machines drives, digital control of static converters in different applications including microgrids.

Ralph M. Kennel (M'89–SM'96) received the Diploma and the Dr.-Ing. degree from the University of Kaiserslautern, Kaiserslautern, Germany, in 1979 and 1984, respectively, in power electronics for his work on the application of model predictive control.

From 1994 to 1999, he was a Visiting Professor with the University of Newcastle-upon-Tyne, Tyne and Wear, U.K. From 1999 to 2008, he was a Professor with the Faculty of Electrical Machines and Drives, Wuppertal University, Wuppertal, Germany. Since 2008, he has been a Professor with the Institute for Electrical Drive Systems and Power Electronics, Department of Electrical and Computer Engineering, Technical University of Munich, Munich, Germany. His research interests include sensorless control of alternating-current drives, predictive control of power electronics, and hardware-in-the-loop systems.

Dr. Kennel is a Fellow of the Institution of Electrical Engineers, U.K., and is a Chartered Engineer in the U.K. Within the IEEE, he is the Treasurer of the Germany Section and the Energy Conversion Congress and Exposition Global Partnership Chair of the Power Electronics Society (PELS).